# Biophysical characterization of the oligomeric states of recombinant Immunoglobulins type-M and their C1q binding kinetics by Biolayer Interferometry

**Anne Chouquet[1], Andrea J. Pinto[1], Julia Hennicke[2], Wai Li Ling[1], Isabelle Bally[1], Linda Schwaigerlehner[2], Nicole M. Thielens[1], Renate Kunert[2], Jean-Baptiste Reiser[1,*]**

[1] Institut de Biologie Structurale, UMR 5075, Univ. Grenoble Alpes, CEA, CNRS, IBS, F-38000 Grenoble, France

[2] Department of Biotechnology, University of Natural Resources and Life Sciences, Muthgasse 18, 1190 Vienna, Austria

*** Correspondance:**
Jean-Baptiste Reiser
jean-baptiste.reiser@ibs.fr

**Keywords: Immunoglobulins, IgM, complement, C1q, recombinant expression, biophysical characterization, protein-protein interactions, biolayer interferometry**

**Abstract**

The Immunoglobulins type-M (IgMs) are one of the first antibody classes mobilized during immune responses against pathogens and tumor cells. Binding to specific target antigens enables the interaction with the C1 complex which strongly activates the classical complement pathway. This biological function is the basis for the huge therapeutic potential of IgMs but due to their high oligomeric complexity, *in vitro* production, biochemical and biophysical characterizations are challenging. In the present study, we present recombinant production of two IgM models (IgM617 and IgM012) in pentameric and hexameric states and the evaluation of their polymer distribution using different biophysical methods (AUC, SEC-MALLS, Mass Photometry and Transmission Electron Microscopy). Each IgM oligomer has individual specific expression pattern and yield with different protein quality likely due to intrinsic IgM properties and patterning. Nevertheless, the purified recombinant IgMs retain their ability to activate complement in a C1q dependent manner. And more importantly, a new method to evaluate their functional quality attribute by characterizing the kinetics of C1q binding to recombinant IgM has been developed using BioLayer Interferometry (BLI). We show that recombinant

IgMs possess similar C1q binding properties as IgMs purified from human plasma.

## 1 Introduction

Since their discovery over a century ago, immunoglobulins (Igs) are considered to be one of the main components of the vertebrate humoral immune responses representing the first line of host protection against pathogens and altered-self cells, immune surveillance and homeostasis by recognizing and binding specific antigens. Immunoglobulins of type M (IgMs) are the first Igs produced and secreted by B cells in early infection and immune reaction stages in adults. They are highly oligomeric polypeptides composed of a heavy chain (H) and a light chain (L). Each chain contains an N-terminal variable domain and one (for the L chain) or four (for the H chain) C-terminal constant domains. IgMs are found as assembly of $H_2L_2$ protomer subunits either in a pentameric form $(H_2L_2)_5$, containing an additional covalently linked peptide called the Joining (J) chain or, to a minor extent (less than 5%), in hexameric form $(H_2L_2)_6$, devoid of J chain (for reviews Gong and Ruprecht, 2020; Jones et al., 2020; Keyt et al., 2020). IgM are also highly glycosylated with 5 to 6 different N-linked glycosylation chains that can represent up to 10 to 15% of their total molecular weight (Arnold et al., 2005). The overall assembly of IgMs is now revealed by modern high resolution Electron Microscopy (EM) methods: they have been observed as star-shaped structures with a compact Fc core and orbiting, labile and flexible Fab arms. While the hexamers appear to have the expected 6-fold symmetry, the pentamers possess a pseudo-hexameric symmetry where five IgM protomers occupy five of the six symmetric positions and the J chain the sixth position (Hiramoto et al., 2018; Li et al., 2020; Kumar et al., 2021).

In addition to their antigen recognition function, IgMs fulfill their immune effector function as one of the strongest activators of the classical pathway of the complement system. The binding of complexes between specific surface-exposed antigens and IgMs to the first recognition component of the classical pathway (CP), the C1q molecule, initiates complement-dependent cytotoxicity, a regulated amplifying proteolytic cascade which enables the membrane attack complex formation and the elimination of the

50 pathogen or infected cell targets (Ricklin et al., 2010; Cedzyński et al., 2019). Found in high
51 concentration in human serum, C1q, which forms the CP initiation C1 complex together with the pro-
52 enzyme tetramer $C1r_2C1s_2$, is a 460kDa and highly flexible glycoprotein assembled from 18
53 polypeptide chains of 3 types (A, B, C). It is organized into six ABC heterotrimers forming six Ig
54 recognition domains, the globular heads (gC1q), attached to collagen-like regions (CLR) allowing the
55 assembly of what has been depicted as a "bouquet of tulips" or an "Eiffel-tower" (Kishore and Reid,
56 2000; Diebolder et al., 2014; Sharp et al., 2019).

57 Interaction studies of C1q with its Ig ligands led to the recent structures of Ig/C1 complexes by cryo-
58 electron tomography and microscopy that finally revealed the general assembly of the CP initiation
59 step and confirmed some, but not all, of the different biochemical studies performed to characterize the
60 C1q/Ig binding properties and to identify the C1q/Ig binding sites (Ugurlar et al., 2018; Sharp et al.,
61 2019). However, methods to measure the direct binding characteristics of C1q to Igs as functional
62 quality attributes are rather limited in number (reviewed in Harboe et al., 2011). Traditional methods
63 employ Enzyme-Linked Immunosorbent Assays (ELISA) to measure equilibrium and end-point
64 deposition of Igs over coated C1q and vice-et-versa (exemplified in Duncan and Winter, 1988; Idusogie
65 et al., 2000). More recently, label-free and real-time methods such as traditional Surface Plasmon
66 Resonance (SPR) or novel BioLayer Interferometry (BLI) have been used to characterize the binding
67 kinetics between C1q and IgGs (Moore et al., 2010; Patel et al., 2015; Zhou et al., 2018) or IgMs (Bally
68 et al., 2019).

69 In the present study, we report (i) productions of our IgM models, IgM617 and IgM012 in pentameric
70 and hexameric forms (ii) their biochemical and functional quality characterization using Analytical
71 UltraCentrifugation (AUC), Size Exclusion Chromatography coupled to Multi-Angle Laser Light
72 Scattering (SEC-MALLS), Mass Photometry (MP), Transmission Electron Microscopy (TEM) and in-
73 house ELISA-like for detection of complement activation and (iii) the development of protocols to

74 evaluate their bindings to C1q with BLI and to compare their kinetics characteristics.

## 75 2 Materials and Methods

### 76 2.1 IgM genetic constructs

77 IgM617 is originally expressed by the EBV-transformed B cell line HB617 and directed against
78 glycosphingolipids overexpressed on the tumor cell surfaces and elicits cytotoxic T-cells (Vorauer-Uhl
79 et al., 2010). IgM012 was developed after a class switch of a human IgG broadly-neutralizing HIV and
80 is directed against the HIV1 envelope protein gp120 and in particular the carbohydrate mannose
81 structure (Wolbank et al., 2003). All Light chains (L), Heavy chains (H) and Joining chain (J) cDNA
82 of both IgM models were codon-optimized and sub-cloned into separate pIRES vectors as described
83 in Chromikova *et al.* (Chromikova et al., 2015b), into pCEP4 vectors as described in Hennicke *et al.*
84 (Hennicke et al., 2017) and into pcDNA3.1(+) vectors. For the last constructs, IgM chain cDNAs were
85 amplified by PCR using conventional protocols and the pIRES constructs as templates. Additional
86 flanked NheI and BamHI restrictions sites were also introduced by Polymerase Chain Reaction (PCR).
87 The genes were then inserted individually with classical ligation techniques into pcDNA3.1(+) vectors
88 (Invitrogen) containing a resistance cassette for either Geneticin (H chain), Zeocin (L chain) or
89 Hygromycin (J chain).

### 90 2.2 Cell lines and expression of IgM models

91 IgM617-HLJ and IgM012-HLJ forms were expressed using either (i) CHO DG44 cell lines after co-
92 transfection with pIRES constructs and generation of stable cells lines as described in Chromikova *et*
93 *al.* (Chromikova et al., 2015b), (ii) HEK293E cell lines after co-transfection with pCEP4 vectors and
94 transient expression as described in Hennicke *et al.* (Hennicke et al., 2019) or (iii) HEK293F after co-
95 transfection or serial transfections with pcDNA3.1(+) vectors and generation of stable cell lines.
96 Transfection and cultivation conditions of CHO DG44 and HEK293E cell lines have been described
97 previously (Chromikova et al., 2015b; Hennicke et al., 2020). To generate stable IgM-expressing

98 HEK293F cell lines, cells were grown in FreeStyle 293 expression medium and first co-transfected
99 with H-chain- and L-chain-containing pcDNA3.1(+) plasmids using 293fectin according to the
100 manufacturer's protocol (Invitrogen). Stable transfectants producing either IgM617-HL or IgM012-
101 HL were generated using cultivation in medium supplemented with 400 µg/ml G418 (Invitrogen) and
102 10 µg/ml Zeocin (Invitrogen). These cells were then transfected with J-chain-containing pcDNA3.1(+)
103 plasmids in the same way and the stable transfectants producing either IgM617-HLJ or IgM012-HLJ
104 were generated using cultivation in medium supplemented with additional 100 µg/ml hygromycin
105 (Sigma-Aldrich). The stable cells expressing each IgM construct were then expanded in Freestyle 293
106 expression medium under antibiotic pressures every 3 to 4 days when cell density approached $3.10^6$
107 cells/ml.

108 **2.3 Recombinant IgMs purification**

109 All IgMs were purified from harvested supernatants according to Hennicke *et al.* (Hennicke et al.,
110 2017). Briefly, POROS CaptureSelect™ IgM Affinity Matrix (Thermo Fisher Scientific) was used for
111 affinity chromatography. Culture supernatants were directly applied to packed column and the IgMs
112 were eluted with 1 M Arginine, 2 M $MgCl_2$, pH 3.5 or pH 4.0. The collected fractions were immediately
113 neutralized with 1M Tris pH 8.5. The IgM-containing fractions were then pooled and dialyzed against
114 the next-step equilibration buffer. After concentration and for a second Size Exclusion
115 Chromatography (SEC) step, they were applied on a Superose™ 6 increase 10/300 or 16/600 column
116 (GE Healthcare/Cytiva) equilibrated in 0.1 M sodium phosphate pH 7.4, 0.2 M NaCl or in 0.025 M
117 Tris-Base, 0.137 M NaCl, 0.003 M KCl, pH7.4 at a flow rate of 0.5 mL/min. Highly multimeric IgMs
118 were eluted as a single peak separated from lower or higher oligomeric states and from nucleic acid
119 contaminants. Identification of purified IgMs by SDS-PAGE was performed as described in Vorauer-
120 Uhl *et al.* (Vorauer-Uhl et al., 2010) using Native PAGE 3-12% Bis-Tris gels and followed by
121 Coomassie Blue staining.

122 **2.4 C1q purification from plasma**

123 C1q was purified from human serum according to the well-established protocol published by Arlaud
124 *et al.* (Arlaud et al., 1979).

125 **2.5 Analytical Ultracentrifugation**

126 Sv-AUC experiments were conducted in an XLI analytical ultracentrifuge (Beckman, Palo Alto, CA)
127 using an ANTi-60 rotor and double channel Ti centre pieces (Nanolytics, Germany) of 12- or 3-mm
128 optical path length equipped with sapphire windows, the reference channel being typically filled with
129 the sample solvent. Acquisitions were done overnight at 4°C and at 20000 rpm (32000 g) using
130 absorbance (280 nm) and interference detection. Data processing and analysis were done using the
131 program SEDFIT (Schuck, 2000) from P. Schuck (NIH, USA), REDATE (Zhao et al., 2015) and
132 GUSSI (Brautigam, 2015) from C. Brautigam (USA), and using standard equations and protocols
133 described previously (Salvay et al., 2008; Le Roy et al., 2013, 2015).

134 **2.6 Size Exclusion Chromatography - Multi Angle Laser Light scattering (SEC-MALLS)**
135 **analyses**

136 SEC combined with online detection by MALLS, refractometry and UV-Vis was used to measure the
137 absolute molecular mass in solution. The SEC runs were performed using a Superose$^{TM}$ 6 increase
138 10/300 column (GE Healthcare/Cytiva) equilibrated in 0.025 M Tris-Base, 0.137 M NaCl, 0.003 M
139 KCl, pH 7.4. Separation was performed at room temperature and 50 µl of protein sample, concentrated
140 to about 1 mg/ml, were injected with a constant flow rate of 0.5 ml/min. Online MALLS and
141 differential refractive index detection were performed with respectively a DAWN-HELEOS II detector
142 (Wyatt TechnologyCorp.) using a laser emitting at 690 nm and an Optilab T-rEX detector (Wyatt
143 Technology Corp.), respectively. Weight-averaged molar masses (Mw) determination was done with
144 the ASTRA6, using the "protein conjugate" module of the ASTRA software package. The following
145 refractive index increments and UV-Vis absorbance values were used: *dn/dc* protein = 0.185 mL/g;

146 *dn/dc* glycosylation = 0.15 mL/g; $A_{280}$=1.38 ml/mg.cm.

147 **2.7 Mass Photometry**

148 Coverslips (high precision glass coverslips, 24x50 $mm^2$, No. 1.5H; Marienfeld, Lauda-Königshofen,
149 Germany) were cleaned by sequential sonication in Milli-Q $H_2O$, 50% iso- propanol (HPLC
150 grade)/Milli-Q $H_2O$, and Milli-Q $H_2O$ (5 min each), followed by drying with a clean nitrogen stream.
151 To keep the sample droplet in shape, reusable self- adhesive silicone culture wells (Grace Bio-Labs
152 reusable CultureWell$^{TM}$ gaskets) were cut in segments of 4 to 10. To ensure proper adhesion to the
153 coverslips, the gaskets were dried well by using a clean nitrogen stream. To prepare a sample carrier,
154 gaskets were placed in the center of the cleaned coverslip and fixed tightly by applying light pressure
155 with the back of a pipette tip. Protein landing was recorded using a Refeyn One$^{MP}$ (Refeyn Ltd., Oxford,
156 UK) MP system by forming a droplet of each IgM sample with a final concentration of 10 nM in a
157 buffer solution containing 0.025 M Tris-Base, 0.137 M NaCl, 0.003 M KCl, pH7.4. Movies were
158 acquired for 120 s (12000 frames) with Acquire$^{MP}$ (Refeyn Ltd., v2.1.1) software using standard
159 settings. Contrast-to-mass (C2M) calibration was performed using a mix of proteins with molecular
160 weight of 66, 146, 500, and 1046 kDa. Data were analyzed using Discover$^{MP}$ (Refeyn LTD, v2.1.1)
161 and analysis parameters were set to T1 = 1.2 for threshold 1. The values for number of binned frames
162 (nf = 8), threshold 2 (T2 = 0.25), and median filter kernel (=15) remained constant. The mean peak
163 contrasts were determined in the software using Gaussian fitting. The mean contrast values were then
164 plotted and fitted to a line. The experimental masses were finally obtained by averaging replicates and
165 errors were the standard deviation.

166 **2.8 Transmission electron microscopy (TEM)**

167 About 4 µl of diluted IgM samples (60 to 80 ng) were applied to a carbon film evaporated onto a mica
168 sheet. The carbon film was then floated off the mica in ~100 µL 2 % sodium silicotungstate (SST, Agar
169 Scientific) and transferred onto a 400 mesh Cu TEM grid (Delta Microscopies). Images were acquired

170 with a CETA camera on a Tecnai F20 TEM microscope operating at 200 keV.

171 **2.9 Complement activation-ELISA**

172 The activation of the classical complement pathway was monitored by an ELISA based on the detection
173 of C4b deposition according to Bally *et al.* and Hennicke *et al.*(Bally et al., 2019; Hennicke et al.,
174 2020). Briefly, 200 ng of IgMs were immobilized on a MaxiSorp 96-well plate (Thermo Fisher
175 Scientific) and incubated with Normal Human Serum (NHS) diluted 25 times, C1q-depleted serum
176 (NHSΔ, CompTech) diluted 25 times or NHSΔ diluted 25 times reconstituted with purified human C1q
177 (4 µg/mL). NHS was obtained from the Etablissement Français du Sang Rhône-Alpes (agreement
178 number 14-1940 regarding its use in research). Unspecific binding was prevented by saturation with
179 2% bovine serum albumin (BSA, Sigma Aldrich). Deposited cleaved C4 form was detected with a
180 rabbit anti-human C4 polyclonal antibody (Siemens), an anti-rabbit-HRP antibody conjugate (Sigma
181 Aldrich), addition of TMB (Sigma Aldrich) and a Clariostar plate reader (BMG Labtech). Polyclonal
182 IgM isolated from human serum (Sigma Aldrich) was used as control. Reported values were obtained
183 by normalizing each data set (polyclonal IgM/NHS defined as 100) and by averaging data obtained in
184 replicated independent assays (between 2 to 4); reported errors were the standard deviation of the
185 replicates.

186 **2.10 BioLayer Interferometry**

187 All BLI experiments were performed on an OctetRED96e from Pall/FortéBio and were recorded with
188 the manufacturer software (Data Acquisition v11.1). All protein samples were buffer exchanged
189 against 0.01 M $Na_2HPO_4$, 0.0018 M $KH_2PO_4$, 0.137 M NaCl, 0.0027 M KCl at pH 7.4 (Phosphate
190 Buffer Saline, PBS) or 0.025 M Tris, 0.15 M NaCl, 0.003 M KCL at pH 7.4 (Tris Buffer Saline, TBS)
191 with Zeba Spin Desalting columns (Thermo Fisher Scientific) prior to any loading. Commercial AR2G
192 (amine coupling), SA (streptatividin), APS (aminopropylsilane), Protein A, Protein L biosensors
193 (Pall/FortéBio) or lab-made IgM-specific biosensors were tested. The latter ones, mouse or goat anti-

194 μ chain antibodies (Invitrogen) or CaptureSelect anti-IgM nanobody (Thermo Fisher Scientific) were
195 biotinylated using NHS-PEG4-biotin EZ-link kit (Thermo Fisher Scientific) and captured onto SA
196 biosensors. For capture on AR2G biosensors, IgM samples were diluted in 0.01 M Sodium Acetate at
197 pH 4, 4.5, 5, 5.5 or 6 (best capture at pH 6) and C1q in either 0.01 M Sodium Acetate at pH 4, 4.5, 5
198 or 5.5, 0.01 M MES at pH 6 or 6.5 or 0.01 M HEPES at pH 7 or 7.5 (best capture at pH 7.5); for capture
199 on SA biosensor, IgM or C1q samples were biotinylated using NHS-PEG4-biotin EZ-link kit (Thermo
200 Fisher Scientific) and manufacturer conditions; no chemical treatments were applied before capture on
201 APS, Protein A, Protein L or IgM-specific biosensors. All ligand samples were applied at
202 concentrations between 10 and 50 μg/ml. For association and dissociation, all analyte samples were
203 diluted at concentrations between 10 and 100 nM in TBS complemented with 0.002 M $CaCl_2$ and
204 0.02% Tween-20 as analysis buffer. 0.2 ml of each sample or buffer were disposed in wells of black
205 96-well plates (Nunc F96 MicroWell, Thermo Fisher Scientific), maintained at 25°C and agitated at
206 1000 rpm. Biosensors were pre-wetted in 0.2 ml PBS, 0.02% Tween-20 or analysis buffer for 10 min,
207 followed by equilibration in pre-wetting buffer for 120 s. Biosensors were then loaded with each ligand
208 prepared according to the capture chemistry for between 300 s and 600 s, followed by an additional
209 equilibration step of 120 s or more in analysis buffer. In the cases of AR2G biosensors, they were
210 activated by dipping them in a mix of 10 mM N-hydroxysulfosuccinimide (s-NHS) and 20 mM 1-
211 Ethyl-3-3dimethylaminopropyl (EDC) for 300 s prior capture and quenched with 1M Ethanolamine
212 pH8.5 for 300 s after capture. In the case of APS biosensors, they were quenched with 50 μg/ml BSA
213 solution for 600 s. Association phases were monitored during dipping the functionalized biosensors in
214 analyte solutions for between 180 s and 300 s, and the dissociation phases monitored in analysis buffer
215 for between 180 s and 300 s. To assess and monitor unspecific binding of analytes, analyses were
216 performed with biosensors treated with the same protocols but replacing ligand solutions by analysis
217 buffer. Kinetics analyses were performed using Protein L biosensors which were functionalized with

218 each IgM sample diluted at 30 µg/ml for 600 s until reaching a spectrum shift between 5.5 and 7.0 nm.
219 Association phase of plasma C1q was monitored for 300 s with concentrations between 0 and 100 nM
220 and dissociation phase for 600 s. All measurements were performed in replicates with independent IgM
221 loadings. Kinetics data were processed with the manufacturer software (Data analysis HT v11.1).
222 Signals from reference biosensor and zero-concentration sample were subtracted from the signals
223 obtained for each functionalized biosensor and each analyte concentration. Resulting specific kinetics
224 signals were then fitted using a global fit method and 2:1 heterogeneous ligand model. Reported
225 kinetics parameter values were obtained by averaging the values obtained with replicated assays
226 (between 2 to 4) and reported errors as the standard deviation.

227 **3 Results**

228 **3.1 Expression by HEK293F and purification of recombinant IgM in different oligomeric**
229 **forms**

230 Previously, the production of recombinant IgM models using different mammalian expression systems
231 was intensively studied in stable and transient expression (Wolbank et al., 2003; Vorauer-Uhl et al.,
232 2010; Chromikova et al., 2015b, 2015a; Hennicke et al., 2017, 2019, 2020). Here, we present an
233 additional production system for the two IgM constructs, IgM617 and IgM012, using stabilized
234 HEK293F cell lines. cDNA of H, L and J chains from both models have been individually subcloned
235 in pcDNA3.1(+). To obtain IgM samples in pentameric forms (IgM617-HLJ and IgM012-HLJ),
236 HEK293F cells were transfected with the three H, L and J pcDNA3.1(+) constructs, while to obtain
237 IgM samples in hexameric forms (IgM617-HL and IgM012-HL), cells were transfected with only H
238 and L vector constructs. After selection and culture expansion, recombinant IgMs were purified from
239 culture media using the optimized protocol established by Hennicke *et al.* (Hennicke et al., 2017). As
240 previously observed in other cell lines, the retrieved yields and sample qualities after purification differ
241 from one recombinant IgM to the other one with higher product titers for IgM617 than IgM012. Indeed,
242 the final purified yield from stable HEK293F culture media of IgM617-HLJ or IgM617HL (5 to 10

243 mg/l of culture supernatant) is 25 to 100 times higher than that of IgM012-HLJ or IgM012-HL (less
244 than 0.1 mg/l of culture supernatant). Furthermore, the production yield and sample quality of IgM617
245 appear reproducible from different cell cultivations and are far more variable for IgM012s and often,
246 samples suffer from low amounts of product and homogeneity.

## 247 3.2 Biophysical characterization of the oligomeric forms of recombinant IgMs

248 The oligomeric distribution and quality of purified IgM samples expressed by HEK293F cell lines were
249 investigated with biochemical, biophysical and structural methods when feasible.

### 250 3.2.1 SDS-PAGE

251 Semi-native PolyAcrylamide Gel Electrophoresis (PAGE) adapted from Vorauer *et al.* (Vorauer-Uhl
252 et al., 2010) shows that purified IgM617-HLJ migrates as a single and homogeneous band while
253 IgM617-HL migrates in a more heterogenous manner with two major bands in the highest molecular
254 weight range, suggesting thus the presence of different high oligomeric states in the absence of J chain
255 (**Figure 1A**). Interestingly, and while IgM012-HLJ and IgM012-HL behave similarly to IgM617
256 constructs, noticeable additional bands at molecular weights below 150 kDa are still observed,
257 suggesting the presence of lower oligomeric states (**Figure 1B**) similarly to what has been described
258 by Chromikova *et al.* (Chromikova et al., 2015b) and Hennicke *et al.* (Hennicke et al., 2020) for the
259 production of IgM617 and IgM012 pentamers in CHO DG44 or HEK239E cell lines.

### 260 3.2.2 SEC-MALLS and AUC

261 To further characterize IgM617-HLJ and IgM617-HL homogeneities, Multi-Angle-Light Scattering
262 coupled to Size Exclusion Chromatography (SEC-MALLS) and sedimentation velocity Analytical
263 Ultra-Centrifugation (sv-AUC) were performed.

264 SEC-MALLS analyses gave a homogeneous sharp peak of about 895 kDa for IgM617-HLJ which falls
265 in the range of theoretical molecular weight of the glycosylated pentamers (891 kDa of amino acids +
266 10 to 15% of glycosylation) (**Table 1** and **Figure 2B**). Surprisingly, a single mass of 947 kDa is also

267 observed for IgM617-HL (**Table 1** and **Figure 2A**), while the construct was anticipated by SDS-PAGE
268 analysis to be a mixture of pentamers and hexamers (see above). The observed mass may likely
269 correspond to average molecular weights from the different glycosylated oligomers (hexamers: 1050
270 kDa; pentamers without J chain: 875 kDa + 10 to 15%). They might thus co-elute as a single peak from
271 SEC and the resolution of this method is not sufficient to separate hexamers and pentamers. To further
272 explore sample heterogeneities, sv-AUC experiments were performed. Migration in the velocity field
273 of IgM617-HLJ samples showed one main homogeneous peak at a sedimentation coefficient of about
274 19 S (more than 75 %) and minor peaks at 12 S (12 %) and 6 S (9 %), revealing the presence of a
275 majority of pentamers but also presence of lower molecular weight oligomers (**Table 1** and **Figure**
276 **2D**). Migration of IgM617-HL samples appeared to be even more heterogeneous with two main peaks
277 at about 21 S (between 60 to 70 % depending of lots) and about 17.5 S (25 to 30 %), which may
278 correspond to hexamers and pentamers, respectively; and two minor peaks at 15.0 S (5 %) and below
279 5 S (3 to 10 %), also lower molecular weight oligomers (**Table 1** and **Figure 2C**). Our AUC data on
280 recombinant IgMs are perfectly in agreement with the sedimentation coefficients originally measured
281 by Eskeland *et al.* in 1975 (Eskeland and Christensen, 1975) on purified IgM from patient sera with or
282 without J chain.

283 **3.2.3 Mass Photometry**

284 To assess more precisely their oligomeric states and experimental molecular masses, IgM samples were
285 further analyzed using an emerging technique enabling accurate native mass measurements of single
286 molecules in solution, the Mass Photometry (MP) (Sonn-Segev et al., 2020). A single population with
287 an average mass of 998 +/- 6 kDa (mean +/- SD over replicates) can be observed for IgM617-HLJ
288 (**Table 1** and **Figure 3B**). The experimental mass matches the mass of fully glycosylated pentamers
289 (891 kDa + 10 to 15% glycosylation). By contrast, IgM617-HL data show several mass populations: 3
290 main populations at 1250 +/- 54 kDa, 1050 +/- 43 kDa, and 841 +/- 37 kDa (**Table 1** and **Figure 3A**)
291 that may correspond to hexamers (1050 kDa + 10 to 15% glycosylation), pentamers (875 kDa + 10 to

292 15%) and tetramers (700 kDa + 10 to 15%), respectively. Minor populations can also be observed and
293 might correspond to lower oligomeric protomer states. This is in agreement with our sv-AUC
294 observation of a mixture of IgM617-HL oligomers (see above). However, the oligomeric distributions
295 appear different and might be accountable for by the usage of different lots of IgM617-HL for the
296 measurements but also by the methods used. IgM012-HLJ appears with a quite homogeneous
297 experimental mass of 944 +/- 32 kDa, corresponding to pentamers (878 kDa + 10 to 15%) although a
298 broad mass distribution is still observed and an additional population at low molecular weight is present
299 and may correspond to the lower oligomeric states (**Table 1** and **Figure 3D**). Finally, IgM012-HL
300 behaves similarly to IgM617-HL with 2 main populations at 1166 +/- 21 kDa and 1052 +/- 34 kDa
301 corresponding to hexamers (1035 kDa + 10 to 15%), and pentamers (862 kDa + 10 to 15%), but low
302 oligomeric states can also be observed (**Table 1** and **Figures 3C**).

303 **3.2.4 Transmission Electron Microscopy**

304 The structural integrity and oligomeric states of IgMs produced by HEK293F were also examined and
305 confirmed with negative staining Transmitted Electron Microscopy (TEM). IgM617-HLJ (**Figure 4B**)
306 and IgM012-HLJ (**Figure 4D**) produced in HEK293F exhibit very similar structural characteristics as
307 previously observed for pentamers produced in HEK293E and CHO DG44, with a central circular core
308 with projecting flexible Fab units in a star-shaped manner as well-known for IgMs isolated from human
309 serum. As expected from biophysical data described above, IgM617-HL (**Figure 4A**) and IgM012-HL
310 (**Figure 4C**) present distinct types of particles: some with a symmetric shape and six arms, confirming
311 the hexameric structural features of HL samples in addition to the pentamer ones, which is also
312 confirmed by particles with an asymetric shape to which five arms can be attributed. As a remark, IgM
313 molecules with lower oligomeric states observed with Mass Photometry and AUC could not be easily
314 identified in TEM micrographs.

315 Taken together, the usage of several biophysical characterization methods allows to show that the

316 retrieved production yields and protein quality in terms of homogeneity and oligomer distribution differ
317 significantly depending on individual recombinant IgM construct. Our presented data confirmed
318 expression of a majority of pentameric IgM in stable HEK293F cell lines transfected with the 3 IgM
319 genes. When only H and L chain genes are transfected to obtain stable HEK293F cells, we also
320 observed the formation of hexamers in addition to pentamers, likely missing the J chain. However,
321 hexamer ratio appears to be variable and appearance of incomplete polymers can be observed in the
322 HL sample preparations.

### 323 3.3 C1q-dependent complement activation by recombinant oligomeric IgM forms produced by 324 HEK293F cells

325 The capacity of the different recombinant IgM preparations to activate CP was analyzed using our in-
326 house *in vitro* Enzyme-Linked Immunosorbent Assay (ELISA) based on the detection of C4b fragment
327 deposition after serum cleavage of C4 by the C1 complex bound to coated IgM molecules (Bally et al.,
328 2019; Hennicke et al., 2020). Assays with C1q-depleted normal human serum and C1q-reconstituted
329 serum were used as controls for the C1q/IgM interaction dependency. Polyclonal IgMs purified from
330 human plasma (pIgMs) were used as positive control and standard. As observed with our previous
331 IgM617 and IgM012 productions (Hennicke et al., 2020), no meaningful differences are observable in
332 the C4b deposition yields between the different coated IgM samples, either serum-derived or
333 recombinant. Thus, the polymer distributions, might not influence the ability of IgMs to activate the
334 proteolytic complement cascade through C1 when coated to the ELISA surfaces (**Figure 5**).

### 335 3.4 C1q binding kinetics to IgMs measured by BLI

336 In order to characterize the binding kinetics of IgMs to C1q, we developed new protocols using a label-
337 free optical method based on the Reflectometric Inference Spectroscopy (RIfS) (Hänel and Gauglitz,
338 2002; Gauglitz, 2020) and its setup known as BioLayer Interferometry (BLI) (Abdiche et al., 2008;
339 Sultana and Lee, 2015) on an OctetRED96e instrument. During the course of this study, plasma

340 purified C1q and plasma-derived IgM preparations or recombinant IgM constructs produced in
341 HEK293F, complemented with IgMs produced in CHO-DG44 and HEK293E (Hennicke et al., 2020)
342 were used. Real-time detection of binding events at the surface of biosensors enables two strategies:
343 (i) using C1q captured as ligand to the biosensor surfaces and the IgMs as analytes or (ii) IgMs captured
344 as ligands to the biosensor surfaces and C1q as the analyte.

345 The first strategy has been evaluated with C1q as ligand either amine coupled onto AR2G biosensors
346 or captured by Streptavidin (SA) biosensors after biotinylation. However, although high C1q densities
347 can be reached (3 to 7 nm spectral shift), no binding responses can be retrieved with plasma IgM
348 samples (**Supplementary Figure S1**).

349 In the second strategy, we tested several different commercial biosensors (AR2G, SA, APS, Protein A
350 and Protein L) and lab-made IgM-specific biosensors (mouse or goat anti-μ chain antibodies or
351 CaptureSelect anti-IgM nanobody coated on SA biosensors). All biosensors could be functionalized
352 with plasma-derived polyclonal IgMs at different high levels depending of the capture chemistry
353 (between 1 to 7 nm spectral shift) (**Supplementary Figure S2 left panels, Figure S3B**). Since Protein
354 A is specific to Fcγ regions of IgG but also to $VH_3$ subfamilies of Ig, both monoclonal recombinant
355 IgM617 and IgM012 have been tested but no capture signal could be retrieved for this type of
356 biosensors although IgM617 belongs to the $VH_3$ subfamily. Unspecific binding of C1q was also
357 evaluated for all biosensor types: without any captured IgM, most of them showed either low or no
358 unspecific signals from C1q, contrary to what was previously reported (Zhou et al., 2018)
359 (**Supplementary Figures S2 right panels**). Finally, either no or too weak C1q binding signals can be
360 retrieved from most of the IgM-functionnalized biosensors, making them not applicable kinetics and
361 affinity determination (AR2G, SA, Protein A, APS, anti-μ chain antibodies) (**Supplementary Figure**
362 **S2 right panels**). Only protein L biosensors show both limited signals of unspecific C1q binding
363 (**Supplementary Figure S3A**) and measurable kinetics signals on the IgM-functionalized biosensors.

364 Thus, pIgMs, IgM617 and IgM012 constructs were stably absorbed on Protein L biosensors until
365 reaching saturation (4 to 7 nm shift) (**Supplementary Figure S3B**) and kinetics analyses were then
366 performed by dipping the IgM-functionalized biosensors in C1q concentration series ranging from 3.13
367 to 100 nM with 2-fold dilution (**Figure 6**).

368 C1q binds to all IgMs in a biphasic manner, with two distinguishable fast and slow binding rates, and
369 the 1:1-Langmuir model could not be applied to determine interaction kinetics parameters. Thus, the
370 only fitting model available to take into account both kinetics components was the 2:1-heterogeneous-
371 ligand model (**Figure 6**). Polyclonal IgMs extracted from plasma and all recombinant monoclonal
372 IgMs show affinities in the nM scale, ranging from about 1 nM to 8 nM for $K_{D1}$ and from 4 to 26 nM
373 for $K_{D2}$, depending on the sample (**Table 1**). Although the differences may not be significant, IgM012s
374 seems to possess slightly better affinity for C1q ($K_{D1}$ = 1 to 3 nM, $K_{D2}$ = 4 to 10 nM) than IgM617s
375 ($K_{D1}$ = 6 to 8 nM, $K_{D2}$ = 7 to 26 nM). They thus behave more similarly to pIgMs ($K_{D1}$ = 2.3 nM, $K_{D2}$ =
376 6.5 nM) than IgM617s. It has to be noted that for all IgM samples, both distinguishable slow and fast
377 kinetics lead to affinities in the same nM order of magnitude. No significant differences in kinetics,
378 which could be related to the host cell line, can be observed either for IgM617 or IgM012 models.
379 Finally, although small differences can be noted in kinetics rate values when comparing HL and HLJ
380 constructs, it is difficult to attribute them solely to the presence of hexameric forms, since such
381 variations are also observed either between HLJ constructs or between different preparations of the
382 very same recombinant IgM construct (**Table 1**).

383 **4 Discussion**

384 In the presented study, we recombinantly produced and purified two IgMs models, IgM617 and
385 IgM012 (Hennicke et al., 2017, 2019, 2020) in different oligomeric states and fully characterized their
386 biochemical and functional quality attributes using combined biophysics techniques : (i) AUC, SEC-
387 MALLS, MP and TEM to determine their oligomeric states and polymer distributions, (ii) *in vitro*

388 complement activation based on ELISA to evaluate their functional capacities. Moreover, we
389 developed a new protocol using a label-free and real-time detection technique, the BLI, to quantify the
390 kinetics of the interaction between IgMs and the recognition and activating protein of the classical
391 complement pathway, C1q.

392 One challenge for studying IgM and developing potential therapeutic products is the manufacturing
393 and characterization of recombinant molecules of high quality in terms of Ig productivity,
394 homogeneous oligomerization status, purity and biological biomimetic function. In the past years,
395 several methods have been tested and in particular both IgM617 and IgM012 have been taken as IgM
396 models to develop proof-of-concepts of recombinant production (Vorauer-Uhl et al., 2010; Mader et
397 al., 2013; Chromikova et al., 2015b; Hennicke et al., 2017, 2019, 2020). In the present study, we
398 complemented biophysical sample analysis method panel by using SEC-MALLS (**Figure 2**), sv-AUC
399 (**Figure 2**) and the new MP (**Figure 3**) to determine the oligomeric distribution of recombinant IgM
400 samples produced in HEK293F cell line. We can thus confirm that IgM617-HLJ model can be
401 produced as very homogeneous full pentamers when H, L and J chain genes are transfected in
402 HEK293F for stable expression, while IgM012-HLJ retains heterogeneities with significant amounts
403 of lower oligomers. Despite these challenging behaviors, both IgM pentamers produced in HEK293F
404 retain their structural integrity of five-branches-star-shaped particles (**Figure 4**) as shown with negative
405 staining TEM images and functional qualities as demonstrated with complement activation assays
406 (**Figure 5**). One explanation for the challenging behavior of IgM012 in recombinant expression
407 compared to IgM617 and in general to other IgM constructs studied so far, may come from its origin:
408 it is a class switch of the human monoclonal anti-HIV-1 antibody 2G12 (Wolbank et al., 2003). Indeed,
409 the 2G12 Fab crystal structure revealed an unusual VH-VL domain arrangement for Fabs where two
410 of its Fabs assemble as a dimer with interlocked VH domain swapping, instead of the usual VH-VL
411 monomeric assembly (Calarese et al., 2003). The VH domain exchange has been demonstrated to be

412 mandatory for this IgG to target and to recognize the specific high-mannose cluster of the glycan shield
413 of HIV-1 (Doores et al., 2010). One can easily hypothesize that IgM012 might possess such similar
414 domain swapping of its Fabs and this might constrain IgM assembly more than the regular one in which
415 Fabs behave independently. These structural constraints might not be favorable and might impair a
416 proper expression of the IgM012 recombinant constructs by the different cell lines used so far.

417 With this study, we show that, by stably transfecting HEK293F cells with only the H and L constructs,
418 IgM617-HL, and to a lesser extend IgM012-HL, hexamer expression is made possible using HEK293F.
419 It was well established that the J chain expression influences the formation of the pentameric and
420 hexameric IgM forms either *in vivo* or *in vitro*. Randall *et al.* in 1992 first demonstrated the
421 pentamer/hexamer ratio secretion regulation in B cells by J chain gene expression with the secretion
422 of a majority of hexamers and a minority of pentamers by cells lacking the J chain gene (Randall et al.,
423 1992). However, recombinant expression of only hexamers by J-chain deficient cells remains
424 challenging. Although hexamers were found to be expressed by recombinant systems, a majority of
425 pentamers is found to be secreted by mouse hybridoma cell lines (Wiersma et al., 1998; Collins et al.,
426 2002) or CHO-K1(Gilmour et al., 2008). Interestingly, only Azuma *et al.* succeeded to obtain a
427 majority of hexamers by using CHO-DG44 that expressed 20 times more hexamers that the CHO co-
428 transfected with the J chain gene (Azuma et al., 2007). Here, we confirm that recombinantly producing
429 homogeneous hexameric forms of IgM remains difficult. Although IgM617 and IgM012 models can
430 be expressed and secreted as hexamers by stable HEK293F cell lines as shown by our different
431 biochemical, biophysical and structural analyses, our data also show that both sample types are not
432 homogeneous: they present a large population of pentamers likely lacking the J chain, but also traces
433 of lower molecular weighted oligomers, likely tetramers and dimers, in the purified IgM samples.
434 Moreover, the ratio between the distinct IgM oligomeric states appears not only variable from an IgM
435 model to the other one but also between different production runs of the same IgM model (data not

436 shown). Additionally, our data from our surface-based C1q-dependent complement activation assays
437 do not demonstrate higher activities of IgM samples enriched with hexamers (**Figure 5**). This contrasts
438 with previous hemolytic assays, which demonstrated the higher efficacy of hexameric IgM to induce
439 complement-dependent cytolysis compared to pentameric IgMs (Randall et al., 1990; Collins et al.,
440 2002). As pointed previously, the ELISA-like setup and the end-point measurement of C4 deposition
441 might not be sensitive and resolutive enough to characterize differences in IgM abilities to activate the
442 first activation step of the complement (Hennicke et al., 2020).

443 For the first time, we introduced a new method to characterize the binding kinetics and affinities of
444 C1q to IgM antibody isotypes using BLI. Optical and surface-based methods such as SPR and BLI are
445 popular methods to characterize the binding properties of all antibody classes to antigens, but much
446 less to Ig effectors such as the complement molecule, C1q. Patel *et al.* in 2015 (Patel et al., 2015) and
447 Jovic *et al.* in 2019 (Jovic and Cymer, 2019) have successfully characterized the binding responses of
448 C1q to the different IgG subtypes using traditional SPR methods and Zhou *et al.* in 2018 (Zhou et al.,
449 2018) using the recent BLI technology. Concerning the IgM/C1q interaction properties, a single study
450 has been published by Bally *et al.* in 2019 (Bally et al., 2019) who measured, using SPR, the binding
451 kinetics between IgM fractions purified from human plasma and native C1q, as well as recombinant
452 C1q and a few critical mutants.

453 Several experimental setups have been tested in our study to define the conditions allowing reliable
454 binding measurements between either IgM purified from human plasma or different recombinant IgM
455 constructs and native C1q purified from human plasma. Surprisingly and in contrast to the SPR data
456 obtained so far when C1q is captured at the biosensor surface (Bally et al., 2019), no interaction with
457 IgMs was detectable with the BLI method (**Supplementary Figure S1**). However, we could observe
458 binding of the catalytic tetramer $C1r_2Cs_2$ to immobilized C1q with expected affinities in the nanomolar
459 range (**Supplementary Figure S4**). These results indicate that immobilized C1q can retain certain

460 binding activities towards its partners but that the immobilization strategy to the BLI biosensor either
461 directly or via selective biotinylation of primary amines of C1q can greatly affect its binding capacities.

462 In the course of optimizing the BLI protocols, capturing IgMs on Protein L biosensor and using C1q
463 as analyte has proven to be the most efficient strategy since only low or acceptable unspecific C1q
464 binding can be detected at the used concentration range (**Supplementary Figure S3**) and specific
465 concentration dependent binding signals can be measured (**Figure 6**). Our method meets the ones
466 already employed to characterize the complexes between C1q and recombinant IgGs, for which Protein
467 L coated sensors have been used to capture immunoglobulins for SPR or BLI, although Streptavidin
468 and biotin fusion have also been proven to be suitable (Zhou et al., 2018). Unfortunately, protein L was
469 the only successful immobilization method for functionalizing BLI biosensors with IgMs. Indeed, the
470 binding of protein L to Igs is specifically restricted to certain kappa light chains, which limits the
471 application of the method described here to IgMs containing this subtype of L chain, such as our
472 models. Surprisingly, binding of C1q can be measured in those conditions and without any specific
473 antigen bound to IgMs. Similarly, complement activation can be quantified without antigen with solid
474 phase methods such as ELISA like techniques as shown by our presented and previous data (Bally et
475 al., 2019; Hennicke et al., 2020), while antigen is required in solution methods such as erythrocyte or
476 liposome lysis (for assays review in Harboe et al., 2011). Indeed, it is thought that C1q binding to IgM
477 and subsequent activation of complement cascade are made possible only after IgM binding to specific
478 antigen which induces large structural changes in IgM quaternary structure and the exposure of the
479 cryptic binding sites for C1q globular heads (Sharp et al., 2019). One possible explanation would be
480 that immobilizing IgMs over an *in vitro* surface might somehow provoke the necessary structural
481 feature exposures. In particular for BLI experiments for which only IgM captures via Protein L allow
482 C1q binding, the explanation might come from the binding properties of Protein L to Ig. As shown by
483 the 3D structure of the complex between Protein L and Fab, one Protein L domain bridges two Fab

484 domains (Graille et al., 2001). Although this property may not strictly mimic antigen binding, it might
485 be enough to induce an IgM conformation allowing complex formation with C1q.

486 As expected, the measured affinities of C1q for IgMs with BLI fall within the nM range (**Table 2**). No
487 significant differences in affinities and kinetics rates could be observed between polyclonal IgM
488 purified from plasma and the different monoclonal recombinant IgMs. Together with the complement
489 assays, which also show no differences between IgM samples, our BLI data emphasize that
490 recombinant IgM preparations retain similar abilities as physiological IgMs to bind and to activate the
491 CP *in vitro*. Our data are very consistent with SPR data obtained by Bally *et al.* (Bally et al., 2019).
492 However, the kinetics behavior appears to be different since a 2:1 heterogenous model has been applied
493 to fit our BLI binding data (**Figure 6**), while a 1:1 Langmuir model is sufficient to interpret SPR data.
494 One can argue that the biphasic kinetics behavior might be raised by the heterogenous quality of native
495 or of our recombinant IgM samples. However, no difference is observed between the most
496 homogeneous constructs (*i.e.* IgM617-HLJ) and the other ones. Thus, the differences observed between
497 SPR and BLI data likely originate from the used methods and strategies: the used functionalized
498 sensors have different capture chemistries and captured molecules (Amine coupled C1q in case of SPR,
499 Protein L/IgMs in case of BLI) and different molecules are used as analyte (IgM in case of SPR, C1q
500 in case of BLI). The question will remain unanswered since no binding could be detected with SPR,
501 capturing IgMs on Protein L sensors and using C1q as analyte (data not shown). At last, BLI
502 measurements of the binding between IgMs and C1q might reveal intrinsic behaviors of the complex
503 formation between those highly oligomeric and flexible molecules. It is expected that single globular
504 region of C1q may have a lower affinity for Igs than full C1q, as well as IgM protomer for C1q than
505 full IgM. Thus, the apparent and necessary affinities for the C1q/IgM complex formation rely on the
506 specific multivalency that enhance the binding with an avidity effect. Furthermore, a certain liability
507 of the C1q/Ig complex formation has been observed: not all gC1q bind the IgG hexamers at the same

508 time (Ugurlar et al., 2018), although the same behavior has not been described for IgMs (Sharp et al.,
509 2019). Finally, because of the very high flexibility of IgM and C1q molecules, structural arrangements
510 and stabilization are highly expected during the binding events. All taken together, these molecular
511 characteristics would induce very complicated and heterogenous binding kinetics for which any
512 mathematical fitting model would not be sufficiently formulated and easily applied to consider all
513 possible behaviors.

514 As a conclusion, our work presents relevant results for the development of IgM as biopharmaceuticals,
515 which requires new *in vitro* methods to produce biosimilars and to characterize the quality attributes
516 of recombinant samples to meet the regulations of various drug and health authorities around the world.
517 For antibodies, non-clinical studies must be performed to assess first the product qualities in terms of
518 purity and homogeneity. Electrophoresis has been widely used so far but with the known limitations
519 in detecting low protein amounts and the application of particular protocols necessary to characterize
520 high molecular-weight biomolecules such as IgMs (Vorauer-Uhl et al., 2010). Our results showed the
521 relevance of additional biophysical methods to precisely determine oligomeric distributions and the
522 molecular weight of different IgM sample states. In particular, Mass Photometry appeared to be a
523 reliable technique to assess rapidly the mass distribution with minimal sample amounts. The
524 characterization of the similarity in known Fab- and Fc-associated functions such as binding to target
525 antigen(s) and to Fc gamma receptors, FcRn or C1q are challenging, in particular in finding methods
526 to demonstrate the binding of Igs to C1q. For now, the characterization of the latter case by ELISA
527 have been widely used in pharmaceutical industry as a surrogate to complement dependent cytotoxicity
528 assays in comparability studies for therapeutic Igs. Optical surface-based methods such as SPR and
529 BLI have been proven to be alternatives with advantages like lower complexity in buffer preparations,
530 lower hands-on manipulation, lower sample consumptions and to be faster, more in-depth and semi-
531 automated Ig/C1q interaction analysis methods with higher precisions than the endpoint measurements

532 from ELISA (Patel et al., 2015; Zhou et al., 2018; Jovic and Cymer, 2019). With our study, we
533 demonstrated the suitability of the BLI-based assays for the interaction of recombinant IgM/C1q
534 interactions and we believe that the developed methods and protocols can be easily applied to evaluate
535 future IgM potential therapeutical preparations in combination with the conventional biological
536 analysis.

537 **5 Abbreviations**

538 AUC: Analytical Ultra-Centrifugation

539 BLI: BioLayer Interferometry

540 CLR: Collagen-like region of C1q

541 ELISA: Enzyme-Linked Immunosorbent Assay

542 H/H chain: Heavy chain

543 L/L chain: Light chain

544 gC1q: globular head of C1q

545 Ig/Igs: Immunoglobuline/s

546 IgG/IgGs: Immunoglobuline/s G

547 IgM/IgMs: Immunoglobuline/s M

548 J/J chain: Joining chain

549 ELISA: Enzym-Linked Immunosorbent Assay

550 EM: Electron Microscopy

551 MP: Mass Photometry

552 PCR: Polymerase Chain Reaction

553 RIfS: Reflectometric Interference Spectroscopy

554 SEC: Size Exclusion Chromatography

555 SEC-MALLS: Multi-Angle-Light Scattering coupled to Size Exclusion Chromatography

556 SPR: Surface Plasmon Resonance

557 TEM: Transmitted Electron Microscopy

558 PAGE: PolyAcrylamide Gel Electrophoresis

## 559 6 Acknowledgments

560 cDNA coding for IgM617 and IgM012 chains were provided by Polymun Scientific
561 Immunobiologische Forschung GmbH. This work used the Biophysical, AUC, EM and SPR/BLI
562 platforms of the Grenoble Instruct-ERIC center (ISBG; UAR 3518 CNRS-CEA-UGA-EMBL) within
563 the Grenoble Partnership for Structural Biology (PSB), supported by FRISBI (ANR-10-INBS-0005-
564 02) and GRAL, financed within the University Grenoble Alpes graduate school (Ecoles Universitaires
565 de Recherche) CBH-EUR-GS (ANR-17-EURE-0003). We thank Caroline Mas for her assistance at
566 the Biophysical platform, Christine Ebel and Aline Le Roy at AUC platform. The EM facility is
567 supported by the Auvergne Rhône-Alpes Region, the Fondation pour la Recherche Médicale (FRM),
568 the Fonds FEDER and the GIS-Infrastructures en Biologie Santé et Agronomie (IBiSA). We thank
569 Guy Schoehn, head of EM facility, for his support. IBS acknowledges integration into the
570 Interdisciplinary Research Institute of Grenoble (IRIG, CEA). We would like to thank Véronique Rossi
571 and Christine Gaboriaud from IBS for their expertise, helpful discussions and article proof reading.

## 572 7 Conflict of Interest

573 The authors declare that they have no conflicts of interest with the contents of this article.

## 574 8 Author Contributions

575 Conceptualization & supervision: Jean-Baptiste Reiser, Wai-Li Ling and Renate Kunert

576 Funding acquisition: Nicole Thielens, Jean-Baptiste Reiser and Renate Kunert

577 Investigation and data: Julia Hennicke, Linda Schwaigerlehner and Renate Kunert (for IgM expression
578 and purification in HEK293E and CHO DG44); Isabelle Bally, Anne Chouquet, Andrea Pinto and

Jean-Baptiste Reiser (for IgM expression and purification in HEK293F); Anne Chouquet, Andrea Pinto and Jean-Baptiste Reiser (for Mass Photometry and BLI measurements), Andrea Pinto and Wai-Li Ling (for electron microscopy).

Expertise: Nicole Thielens (for $C1r_2C1s_2$ samples and SPR expertise).

Article writing: Jean-Baptiste Reiser, Wai-Li Ling, Andrea Pinto and Renate Kunert.

## 9 Funding

This work was supported by the French National Research Agency under Grant C1qEffero ANR-16-CE11-0019, the PhD program BioToP (Biomolecular Technology of Proteins) funded by the FWF under Grant W1224 and by Polymun Scientific Immunbiologische Forschung GmbH.

## 10 References

Abdiche, Y., Malashock, D., Pinkerton, A., and Pons, J. (2008). Determining kinetics and affinities of protein interactions using a parallel real-time label-free biosensor, the Octet. *Anal. Biochem.* 377, 209–217. doi:10.1016/j.ab.2008.03.035.

Arlaud, G. J., Sim, R. B., Duplaa, A.-M., and Colomb, M. G. (1979). Differential elution of Clq, C$\bar{1}$r and C$\bar{1}$s from human CT bound to immune aggregates. use in the rapid purification of C$\bar{1}$ sub-components. *Mol. Immunol.* 16, 445–450. doi:10.1016/0161-5890(79)90069-5.

Arnold, J. N., Wormald, M. R., Suter, D. M., Radcliffe, C. M., Harvey, D. J., Dwek, R. A., et al. (2005). Human Serum IgM Glycosylation: IDENTIFICATION OF GLYCOFORMS THAT CAN BIND TO MANNAN-BINDING LECTIN*. *J. Biol. Chem.* 280, 29080–29087. doi:10.1074/jbc.M504528200.

Azuma, Y., Ishikawa, Y., Kawai, S., Tsunenari, T., Tsunoda, H., Igawa, T., et al. (2007). Recombinant Human Hexamer-Dominant IgM Monoclonal Antibody to Ganglioside GM3 for Treatment of Melanoma. *Clin. Cancer Res.* 13, 2745–2750. doi:10.1158/1078-0432.CCR-06-2919.

Bally, I., Inforzato, A., Dalonneau, F., Stravalaci, M., Bottazzi, B., Gaboriaud, C., et al. (2019). Interaction of C1q with pentraxin 3 and IgM revisited: mutational studies with recombinant C1q variants. *Front. Immunol.* 10, 461. doi:10.3389/fimmu.2019.00461.

Brautigam, C. A. (2015). Chapter Five - Calculations and Publication-Quality Illustrations for Analytical Ultracentrifugation Data. *Methods Enzymol.*, 109–133. doi:10.1016/bs.mie.2015.05.001.

Calarese, D. A., Scanlan, C. N., Zwick, M. B., Deechongkit, S., Mimura, Y., Kunert, R., et al. (2003). Antibody Domain Exchange Is an Immunological Solution to Carbohydrate Cluster Recognition. *Science* 300, 2065–2071. doi:10.1126/science.1083182.

610 Cedzyński, M., Thielens, N. M., Mollnes, T. E., and Vorup-Jensen, T. (2019). Editorial: The Role of
611 Complement in Health and Disease. *Front. Immunol.* 10, 1869. doi:10.3389/fimmu.2019.01869.

612 Chromikova, V., Mader, A., Hofbauer, S., Göbl, C., Madl, T., Gach, J. S., et al. (2015a). Introduction
613 of germline residues improves the stability of anti-HIV mAb 2G12-IgM. *Biochim. Biophys. Acta*
614 1854, 1536–1544. doi:10.1016/j.bbapap.2015.02.018.

615 Chromikova, V., Mader, A., Steinfellner, W., and Kunert, R. (2015b). Evaluating the bottlenecks of
616 recombinant IgM production in mammalian cells. *Cytotechnology* 67, 343–356. doi:10.1007/s10616-
617 014-9693-4.

618 Collins, C., Tsui, F. W. L., and Shulman, M. J. (2002). Differential activation of human and guinea
619 pig complement by pentameric and hexameric IgM. *Eur. J. Immunol.* 32, 1802–1810.
620 doi:10.1002/1521-4141(200206)32:6<1802::AID-IMMU1802>3.0.CO;2-C.

621 Diebolder, C. A., Beurskens, F. J., de Jong, R. N., Koning, R. I., Strumane, K., Lindorfer, M. A., et
622 al. (2014). Complement Is Activated by IgG Hexamers Assembled at the Cell Surface. *Science* 343,
623 1260–1263. doi:10.1126/science.1248943.

624 Doores, K. J., Fulton, Z., Huber, M., Wilson, I. A., and Burton, D. R. (2010). Antibody 2G12
625 Recognizes Di-Mannose Equivalently in Domain- and Nondomain-Exchanged Forms but Only Binds
626 the HIV-1 Glycan Shield if Domain Exchanged. *J. Virol.* 84, 10690–10699. doi:10.1128/JVI.01110-
627 10.

628 Duncan, A. R., and Winter, G. (1988). The binding site for C1q on IgG. *Nature* 332, 738.
629 doi:10.1038/332738a0.

630 Eskeland, T., and Christensen, T. B. (1975). IgM Molecules with and without J Chain in Serum and
631 after Purification, Studied by Ultra-centrifugation, Electrophoresis, and Electron Microscopy. *Scand.*
632 *J. Immunol.* 4, 217–228. doi:10.1111/j.1365-3083.1975.tb02620.x.

633 Gasteiger, E., Hoogland, C., Gattiker, A., Duvaud, S., Wilkins, M. R., Appel, R. D., et al. (2005).
634 "Protein Identification and Analysis Tools on the ExPASy Server," in *The Proteomics Protocols*
635 *Handbook* Springer Protocols Handbooks., ed. J. M. Walker (Totowa, NJ: Humana Press), 571–607.
636 doi:10.1385/1-59259-890-0:571.

637 Gauglitz, G. (2020). Critical assessment of relevant methods in the field of biosensors with direct
638 optical detection based on fibers and waveguides using plasmonic, resonance, and interference
639 effects. *Anal. Bioanal. Chem.* 412, 3317–3349. doi:10.1007/s00216-020-02581-0.

640 Gilmour, J. E. M., Pittman, S., Nesbitt, R., and Scott, M. L. (2008). Effect of the presence or absence
641 of J chain on expression of recombinant anti-Kell immunoglobulin M. *Transfus. Med.* 18, 167–174.
642 doi:10.1111/j.1365-3148.2008.00853.x.

643 Gong, S., and Ruprecht, R. M. (2020). Immunoglobulin M: An Ancient Antiviral Weapon –
644 Rediscovered. *Front. Immunol.* 11, 1943. doi:10.3389/fimmu.2020.01943.

645 Graille, M., Stura, E. A., Housden, N. G., Beckingham, J. A., Bottomley, S. P., Beale, D., et al.
646 (2001). Complex between Peptostreptococcus magnus Protein L and a Human Antibody Reveals
647 Structural Convergence in the Interaction Modes of Fab Binding Proteins. *Structure* 9, 679–687.

648 doi:10.1016/S0969-2126(01)00630-X.

649 Hänel, C., and Gauglitz, G. (2002). Comparison of reflectometric interference spectroscopy with
650 other instruments for label-free optical detection. *Anal. Bioanal. Chem.* 372, 91–100.
651 doi:10.1007/s00216-001-1197-3.

652 Harboe, M., Thorgersen, E. B., and Mollnes, T. E. (2011). Advances in assay of complement
653 function and activation. *Adv. Drug Deliv. Rev.* 63, 976–987. doi:10.1016/j.addr.2011.05.010.

654 Hennicke, J., Lastin, A. M., Reinhart, D., Grünwald-Gruber, C., Altmann, F., and Kunert, R. (2017).
655 Glycan profile of CHO derived IgM purified by highly efficient single step affinity chromatography.
656 *Anal. Biochem.* 539, 162–166. doi:10.1016/j.ab.2017.10.020.

657 Hennicke, J., Reinhart, D., Altmann, F., and Kunert, R. (2019). Impact of temperature and pH on
658 recombinant human IgM quality attributes and productivity. *New Biotechnol.* 50, 20–26.
659 doi:10.1016/j.nbt.2019.01.001.

660 Hennicke, J., Schwaigerlehner, L., Grünwald-Gruber, C., Bally, I., Ling, W. L., Thielens, N., et al.
661 (2020). Transient pentameric IgM fulfill biological function—Effect of expression host and
662 transfection on IgM properties. *PLOS ONE* 15, e0229992. doi:10.1371/journal.pone.0229992.

663 Hiramoto, E., Tsutsumi, A., Suzuki, R., Matsuoka, S., Arai, S., Kikkawa, M., et al. (2018). The IgM
664 pentamer is an asymmetric pentagon with an open groove that binds the AIM protein. *Sci. Adv.* 4,
665 eaau1199. doi:10.1126/sciadv.aau1199.

666 Idusogie, E. E., Presta, L. G., Gazzano-Santoro, H., Totpal, K., Wong, P. Y., Ultsch, M., et al.
667 (2000). Mapping of the C1q Binding Site on Rituxan, a Chimeric Antibody with a Human IgG1 Fc.
668 *J. Immunol.* 164, 4178–4184. doi:10.4049/jimmunol.164.8.4178.

669 Jones, K., Savulescu, A. F., Brombacher, F., and Hadebe, S. (2020). Immunoglobulin M in Health
670 and Diseases: How Far Have We Come and What Next? *Front. Immunol.* 11.
671 doi:10.3389/fimmu.2020.595535.

672 Jovic, M., and Cymer, F. (2019). Qualification of a surface plasmon resonance assay to determine
673 binding of IgG-type antibodies to complement component C1q. *Biologicals* 61, 76–79.
674 doi:10.1016/j.biologicals.2019.08.004.

675 Keyt, B. A., Baliga, R., Sinclair, A. M., Carroll, S. F., and Peterson, M. S. (2020). Structure,
676 Function, and Therapeutic Use of IgM Antibodies. *Antibodies* 9, 53. doi:10.3390/antib9040053.

677 Kishore, U., and Reid, K. B. M. (2000). C1q: Structure, function, and receptors.
678 *Immunopharmacology* 49, 159–170. doi:10.1016/S0162-3109(00)80301-X.

679 Kumar, N., Arthur, C. P., Ciferri, C., and Matsumoto, M. L. (2021). Structure of the human secretory
680 immunoglobulin M core. *Structure*, S0969212621000022. doi:10.1016/j.str.2021.01.002.

681 Le Roy, A., Nury, H., Wiseman, B., Sarwan, J., Jault, J.-M., and Ebel, C. (2013). "Sedimentation
682 Velocity Analytical Ultracentrifugation in Hydrogenated and Deuterated Solvents for the
683 Characterization of Membrane Proteins," in *Membrane Biogenesis: Methods and Protocols* Methods
684 in Molecular Biology., eds. D. Rapaport and J. M. Herrmann (Totowa, NJ: Humana Press), 219–251.

685 doi:10.1007/978-1-62703-487-6_15.

686 Le Roy, A., Wang, K., Schaack, B., Schuck, P., Breyton, C., and Ebel, C. (2015). "Chapter Twelve -
687 AUC and Small-Angle Scattering for Membrane Proteins," in *Methods in Enzymology* Analytical
688 Ultracentrifugation., ed. J. L. Cole (Academic Press), 257–286. doi:10.1016/bs.mie.2015.06.010.

689 Li, Y., Wang, G., Li, N., Wang, Y., Zhu, Q., Chu, H., et al. (2020). Structural insights into
690 immunoglobulin M. *Science* 367, 1014–1017. doi:10.1126/science.aaz5425.

691 Mader, A., Chromikova, V., and Kunert, R. (2013). Recombinant IgM expression in mammalian
692 cells: A target protein challenging biotechnological production. *Adv. Biosci. Biotechnol.* 04, 38–43.
693 doi:10.4236/abb.2013.44A006.

694 Moore, G. L., Chen, H., Karki, S., and A, G. (2010). Engineered Fc variant antibodies with enhanced
695 ability to recruit complement and mediate effector functions. *mAbs* 2, 181–189.
696 doi:10.4161/mabs.2.2.11158.

697 Patel, R., Neill, A., Liu, H., and Andrien, B. (2015). IgG subclass specificity to C1q determined by
698 surface plasmon resonance using Protein L capture technique. *Anal. Biochem.* 479, 15–17.
699 doi:10.1016/j.ab.2015.03.012.

700 Randall, T. D., King, L. B., and Corley, R. B. (1990). The biological effects of IgM hexamer
701 formation. *Eur. J. Immunol.* 20, 1971–1979. doi:10.1002/eji.1830200915.

702 Randall, T. D., Parkhouse, R. M., and Corley, R. B. (1992). J chain synthesis and secretion of
703 hexameric IgM is differentially regulated by lipopolysaccharide and interleukin 5. *Proc. Natl. Acad.*
704 *Sci. U. S. A.* 89, 962–966. doi:10.1073/pnas.89.3.962.

705 Ricklin, D., Hajishengallis, G., Yang, K., and Lambris, J. D. (2010). Complement - a key system for
706 immune surveillance and homeostasis. *Nat. Immunol.* 11, 785–797. doi:10.1038/ni.1923.

707 Salvay, A. G., Santamaria, M., le Maire, M., and Ebel, C. (2008). Analytical Ultracentrifugation
708 Sedimentation Velocity for the Characterization of Detergent-Solubilized Membrane Proteins Ca++-
709 ATPase and ExbB. *J. Biol. Phys.* 33, 399. doi:10.1007/s10867-008-9058-3.

710 Schuck, P. (2000). Size-Distribution Analysis of Macromolecules by Sedimentation Velocity
711 Ultracentrifugation and Lamm Equation Modeling. *Biophys. J.* 78, 1606–1619. doi:10.1016/S0006-
712 3495(00)76713-0.

713 Sharp, T. H., Boyle, A. L., Diebolder, C. A., Kros, A., Koster, A. J., and Gros, P. (2019). Insights
714 into IgM-mediated complement activation based on in situ structures of IgM-C1-C4b. *Proc. Natl.*
715 *Acad. Sci.*, 201901841. doi:10.1073/pnas.1901841116.

716 Sonn-Segev, A., Belacic, K., Bodrug, T., Young, G., VanderLinden, R. T., Schulman, B. A., et al.
717 (2020). Quantifying the heterogeneity of macromolecular machines by mass photometry. *Nat.*
718 *Commun.* 11, 1772. doi:10.1038/s41467-020-15642-w.

719 Sultana, A., and Lee, J. E. (2015). Measuring Protein-Protein and Protein-Nucleic Acid Interactions
720 by Biolayer Interferometry. *Curr. Protoc. Protein Sci.* 79, 19.25.1-19.25.26.
721 doi:10.1002/0471140864.ps1925s79.

722 Ugurlar, D., Howes, S. C., de Kreuk, B.-J., Koning, R. I., de Jong, R. N., Beurskens, F. J., et al.
723 (2018). Structures of C1-IgG1 provide insights into how danger pattern recognition activates
724 complement. *Science* 359, 794–797. doi:10.1126/science.aao4988.

725 Vorauer-Uhl, K., Wallner, J., Lhota, G., Katinger, H., and Kunert, R. (2010). IgM characterization
726 directly performed in crude culture supernatants by a new simple electrophoretic method. *J.*
727 *Immunol. Methods* 359, 21–27. doi:10.1016/j.jim.2010.05.003.

728 Wiersma, E. J., Collins, C., Fazel, S., and Shulman, M. J. (1998). Structural and Functional Analysis
729 of J Chain-Deficient IgM. *J. Immunol.* 160, 5979–5989.

730 Wolbank, S., Kunert, R., Stiegler, G., and Katinger, H. (2003). Characterization of Human Class-
731 Switched Polymeric (Immunoglobulin M [IgM] and IgA) Anti-Human Immunodeficiency Virus
732 Type 1 Antibodies 2F5 and 2G12. *J. Virol.* 77, 4095–4103. doi:10.1128/JVI.77.7.4095-4103.2003.

733 Zhao, H., Ghirlando, R., Alfonso, C., Arisaka, F., Attali, I., Bain, D. L., et al. (2015). A
734 Multilaboratory Comparison of Calibration Accuracy and the Performance of External References in
735 Analytical Ultracentrifugation. *PLoS ONE* 10, e0126420. doi:10.1371/journal.pone.0126420.

736 Zhou, W., Lin, S., Chen, R., Liu, J., and Li, Y. (2018). Characterization of antibody-C1q interactions
737 by Biolayer Interferometry. *Anal. Biochem.* 549, 143–148. doi:10.1016/j.ab.2018.03.022.

## 738 11 Figure captions

739 **Figure 1. Semi-native PolyAcrylamide Gel Electrophoresis (PAGE) analysis of purified IgMs**
740 **samples from HEK293F expression.** Native PAGE gels followed by Coomassie Blue staining were
741 run to identify **(A)** IgM617-HLJ and IgM617-HL and **(B)** IgM012-HLJ and IgM012-HL polymer
742 distributions after SEC purification. IgM purified from plasma (Antibodies-onlines) are taken as
743 makers along with Native Markers. Suspected hexamers (H), pentamers (P), dimers (D) and monomers
744 (M) are indicated with arrows.

745 **Figure 2. Size Exclusion coupled to Multi-Angle Light Scattering (SEC-MALLS) and Analytical**
746 **UltraCentrifugation (AUC) analysis of purified IgM617 samples from HEK293F expression.** On
747 the left panels, the chromatograms show the elution profile of the purified **(A)** IgM617-HL and **(B)**
748 IgM617-HLJ monitored by excess refractive index (left ordinate axis) and the molecular weight as bold
749 line (right ordinate axis) derived from MALLS, refractometry and UV-Vis measurements. The
750 estimated average molecular weights are indicated on the graphs. On the right panels, the sedimentation
751 distributions of **(C)** purified IgM617-HL and **(D)** IgM617-HLJ. Calculated and corrected

752 sedimentation coefficients $S_{20,W}$ are obtained as in Materials and Methods and are indicated on the
753 graphs.

754 **Figure 3. Mass Photometry analysis of recombinant IgMs produced in HEK293F.** Histograms
755 show the population distributions of purified IgMs. Shown analyses are representative of replicate
756 experiments: **(A)** IgM617-HL, **(B)** IgM617-HLJ, **(C)** IgM012-HL and **(D)** IgM012-HLJ. Estimated
757 molecular weights for the shown experiments are indicated on each graph.

758 **Figure 4. Non-processed images of negative stain transmission electron microscopy images of**
759 **recombinant IgMs produced in HEK293F.** Representative fields of particles with a 50 nm scale bar
760 on top of each panel and magnified views of some individual molecules are shown on the lower part
761 of each panel: **(A)** IgM617-HL, **(B)** IgM617-HLJ, **(C)** IgM012-HL, **(D)** IgM012-HLJ. Hexamers are
762 denoted with H and Pentamers with P.

763 **Figure 5. Complement activation by the different purified IgMs constructs expressed in**
764 **HEK293F.** Recombinant IgMs and IgMs purified from plasma were coated on microplate wells and
765 incubated with either Normal Human Serum (NHS), C1q-depleted NHS (NHSΔ) or reconstituted NHS
766 (NHSΔ + C1q). C1 activity was monitored via C4b deposition. Reported values are average of
767 replicated (2 to 4) and normalized experiments (100% = IgM plasma/NHS). Errors are obtained as
768 standard deviation between independent replicates.

769 **Figure 6. Kinetics analysis of the interaction between C1q from plasma and the different purified**
770 **and immobilized full IgMs expressed in mammalian expression hosts.** IgMs were captured on
771 Protein L and functionalized biosensors were dipped in wells containing C1q at different
772 concentrations (3.13, 6.25, 12.5, 25, 50, 100 nM). The binding signals (grey-scaled sensorgrams) were
773 obtained by subtracting the signals from empty protein L biosensor and from zero-concentration
774 samples. Fitted curved are depicted as black lines and were obtained by global fitting using a 2:1

775 heterogenous ligand model. Shown kinetics analysis are representative of each binding experiment:
776 **(A)** IgM012-HLJ expressed by CHO DG44, **(B)** IgM617-HLJ by CHO DG44, **(C)** IgM012-HLJ by
777 HEK293E, **(D)** IgM617-HLJ by HEK293E, **(E)** IgM012-HLJ by HEK293F, **(F)** IgM617-HLJ by
778 HEK293F, **(G)** IgM012-HL by HEK293F, **(H)** IgM617-HL by HEK293F, **(I)** IgMs purified from
779 plasma.

780 **12 Table**

781 **Table 1. Summary of theoretical and experiment molecular weights of sedimentation coefficients**
782 **determined by AUC.** The theorical peptide molecular weights are calculated based on the amino-acid
783 primary sequences of the subcloned IgM chains and using Protparam (Gasteiger et al., 2005).
784 Experimental molecular weights were determined by SEC-MALLS and Mass Photometry, coefficient
785 sedimentation by AUC.

786

| IgM | Oligomers | Theoretical (kDa) | SEC-MALLS (kDa) | AUC (S) | Mass Photometry (kDa) |
|---|---|---|---|---|---|
| **IgM617-HL** | **Hexamers** | 1050 | 947 | 21.0 S | 1250 ± 54 |
| | **Pentamers** | 875 | | 17.5 S | 1050 ± 43 |
| | **Tetramers** | 700 | - | 15.0 S | 841 ± 37 |
| | **Dimers** | 175 | - | 5.0 S | 162 ± 12 |
| **IgM617-HLJ** | **Pentamers** | 891 | 895 | 19 S | 998 ± 6 |
| | **Tetramers** | 700 | - | 12 S | - |
| | **Dimers** | 175 | - | 6 S | - |
| **IgM012-HL** | **Hexamers** | 1034 | n.d. | n.d. | 1166 ± 21 |
| | **Pentamers** | 862 | n.d. | n.d. | 1052 ± 34 |
| | **Tetramers** | 690 | n.d. | n.d. | - |
| | **Dimers** | 172 | n.d. | n.d. | 150 ± 21 |
| **IgM012-HLJ** | **Pentamers** | 878 | n.d. | n.d. | 944 ± 32 |
| | **Tetramers** | 690 | n.d. | n.d. | - |
| | **Dimers** | 172 | n.d. | n.d. | 162 ± 14 |

787 (n.d: not determined)

788

789

790 **Table 2. Kinetics and affinity constants of C1q binding to the different purified recombinant**
791 **IgMs expressed in mammalian expression systems.** Values are obtained after global fitting of the
792 binding signals (see Figure 5) and averaging from replicates (2 to 4). Affinity constants ($K_{D1}$ and $K_{D2}$)
793 are obtained from the ratio between kinetics parameters ($k_{d1}/k_{a1}$ and $k_{d2}/k_{a2}$). Standard errors are
794 obtained as standard deviation between replicates.

795

| IgM | Source | Construct | $k_{a1}$ $10^5$/Ms | $k_{d1}$ $10^{-4}$/s | $K_{D1}$ $10^{-9}$ M | $k_{a2}$ $10^7$/Ms | $k_{d2}$ $10^{-1}$/s | $K_{D2}$ $10^{-9}$ M |
|---|---|---|---|---|---|---|---|---|
| **Total IgM** | **plasma** | | 3.04 ± 0.47 | 7.02 ± 1.63 | **2.31 ± 0.09** | 2.00 ± 0.90 | 1.30 ± 0.60 | **6.52 ± 1.34** |
| **IgM617** | **CHO DG44** | **HLJ** | 0.78 ± 0.17 | 6.20 ± 1.02 | **8.00 ± 0.31** | 0.57 ± 0.44 | 0.74 ± 0.08 | **12.30 ± 3.87** |
| | **HEK293E** | **HLJ** | 0.92 ± 0.16 | 6.26 ± 1.77 | **6.82 ± 0.11** | 0.86 ± 0.49 | 0.59 ± 0.33 | **6.90 ± 1.13** |
| | **HEK293F** | **HLJ** | 1.59 ± 0.76 | 11.30 ± 3.04 | **7.10 ± 1.06** | 0.44 ± 0.05 | 1.15 ± 0.53 | **26.4 ± 2.89** |
| | **HEK293F** | **HL** | 1.66 ± 0.50 | 9.25 ± 4.84 | **5.59 ± 1.02** | 0.96 ± 0.38 | 0.96 ±0.47 | **9.97 ± 2.00** |
| **IgM012** | **CHO DG44** | **HLJ** | 2.22 ± 0.08 | 2.57 ± 0.37 | **1.16 ± 0.01** | 2.04 ± 0.31 | 1.34 ± 0.13 | **6.54 ± 0.11** |
| | **HEK293E** | **HLJ** | 1.64 ± 0.35 | 3.57 ± 0.33 | **2.18 ± 0.06** | 1.84 ± 0.40 | 1.57 ± 0.15 | **8.51 ± 0.24** |
| | **HEK293F** | **HLJ** | 2.22 ± 0.33 | 6.18 ± 0.08 | **2.79 ± 0.03** | 1.41 ± 0.34 | 1.34 ± 0.28 | **9.50 ± 0.48** |
| | **HEK293F** | **HL** | 4.65 ± 2.54 | 5.81 ± 2.61 | **1.25 ± 0.31** | 1.79 ± 0.51 | 0.73 ± 0.04 | **4.09 ± 0.17** |

796

# Figure 1

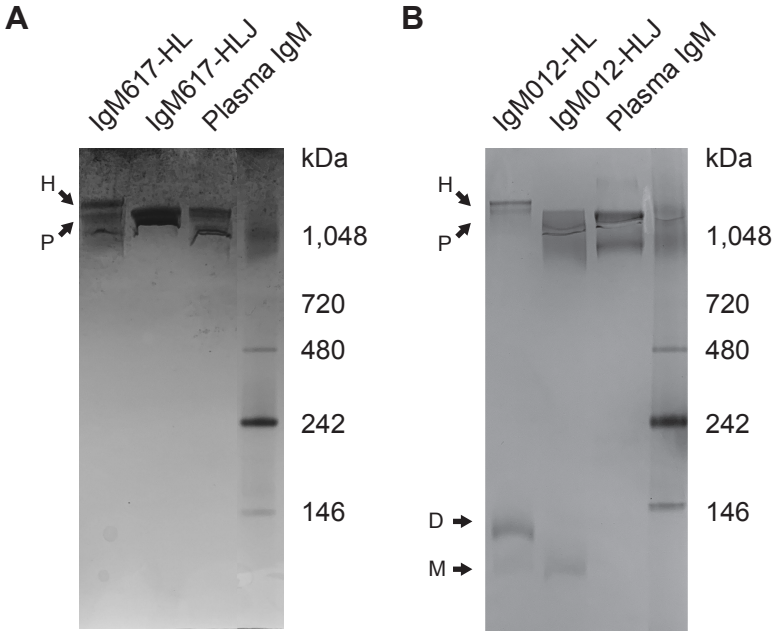
A
IgM617-HL
IgM617-HLJ
Plasma IgM
kDa
H
P
1,048
720
480
242
146
B
IgM012-HL
IgM012-HLJ
Plasma IgM
kDa
H
P
1,048
720
480
242
146
D
M

# Figure 2

## SEC-MALLS

A

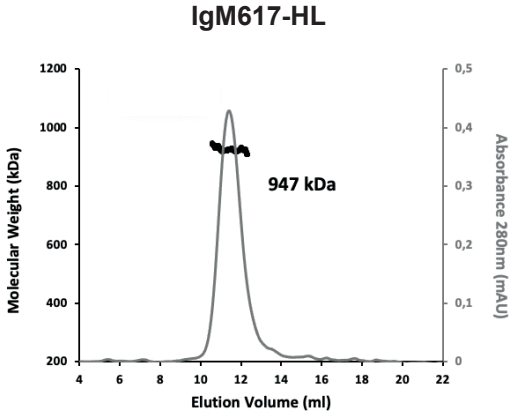


B

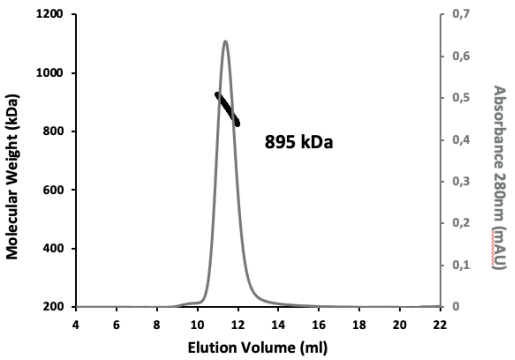


## AUC

C

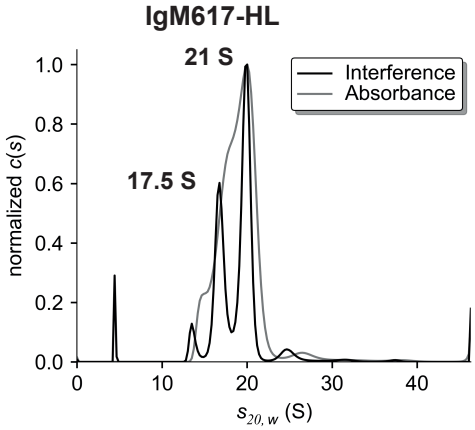


D

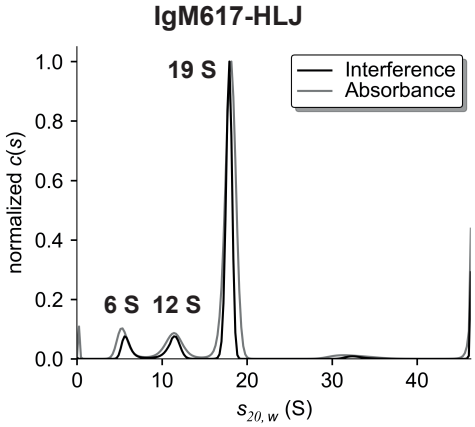

# Figure 3

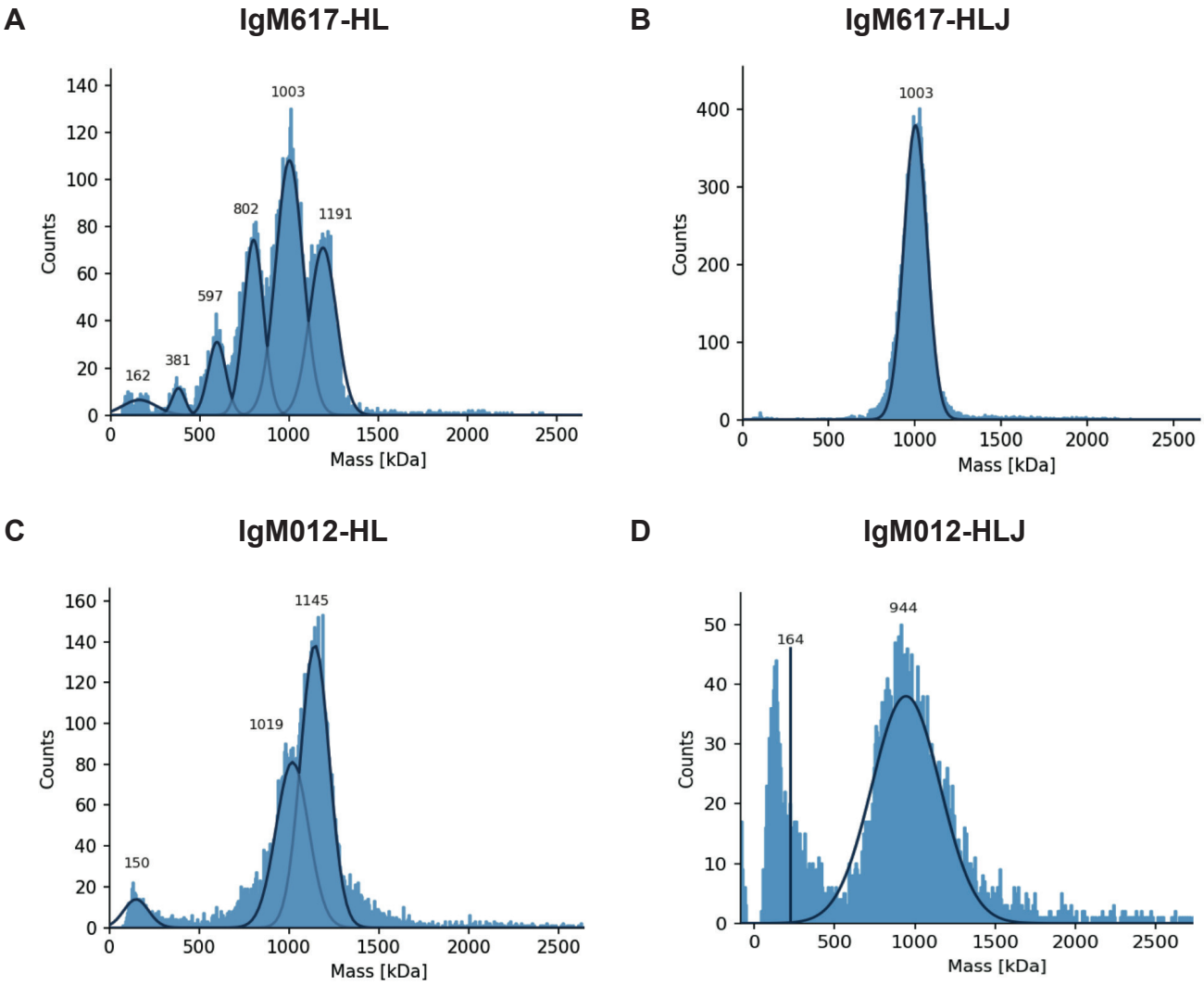
A
IgM617-HL
Counts
Mass [kDa]
162
381
597
802
1003
1191
B
IgM617-HLJ
Counts
Mass [kDa]
1003
C
IgM012-HL
Counts
Mass [kDa]
150
1019
1145
D
IgM012-HLJ
Counts
Mass [kDa]
164
944

# Figure 4

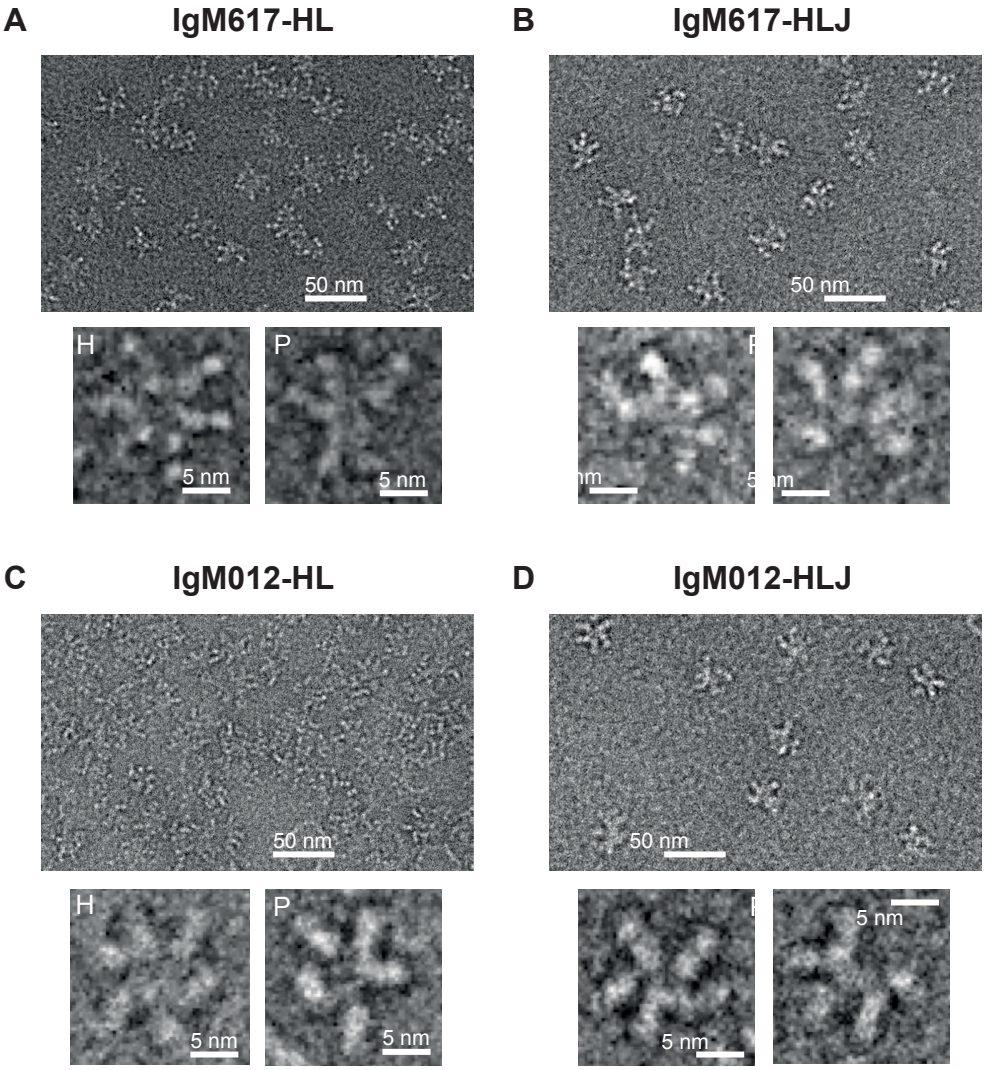
A
IgM617-HL
50 nm
H
5 nm
P
5 nm
B
IgM617-HLJ
50 nm
C
IgM012-HL
50 nm
H
5 nm
P
5 nm
D
IgM012-HLJ
50 nm
5 nm
5 nm

# Figure 5

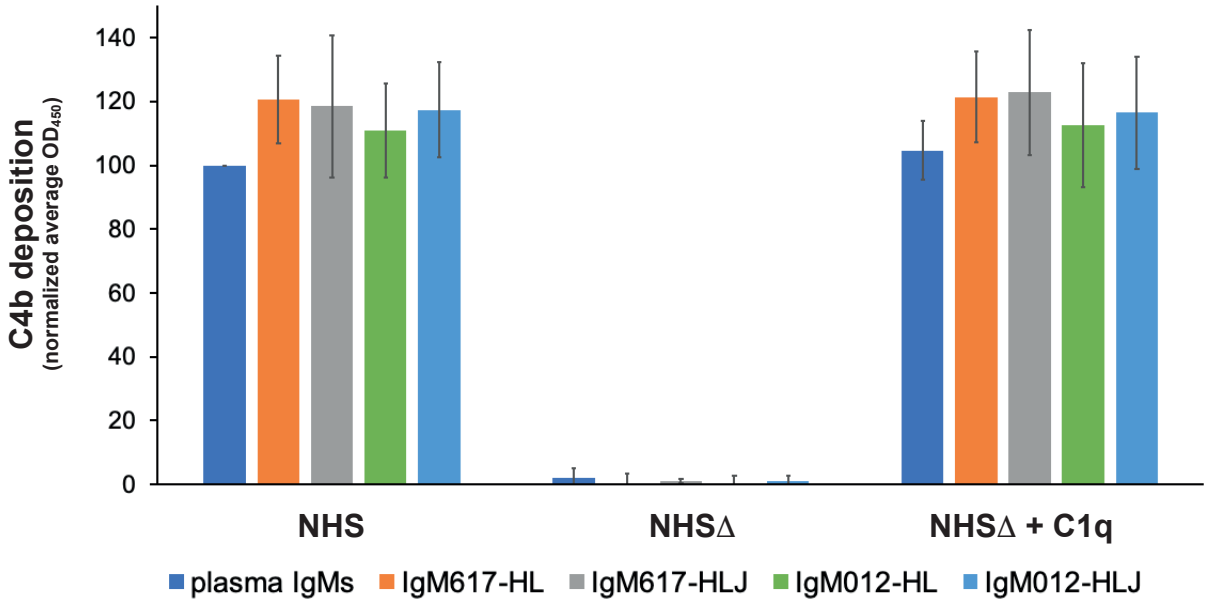
C4b deposition
(normalized average OD450)
140
120
100
80
60
40
20
0
NHS
NHSΔ
NHSΔ + C1q
plasma IgMs
IgM617-HL
IgM617-HLJ
IgM012-HL
IgM012-HLJ

# Figure 6

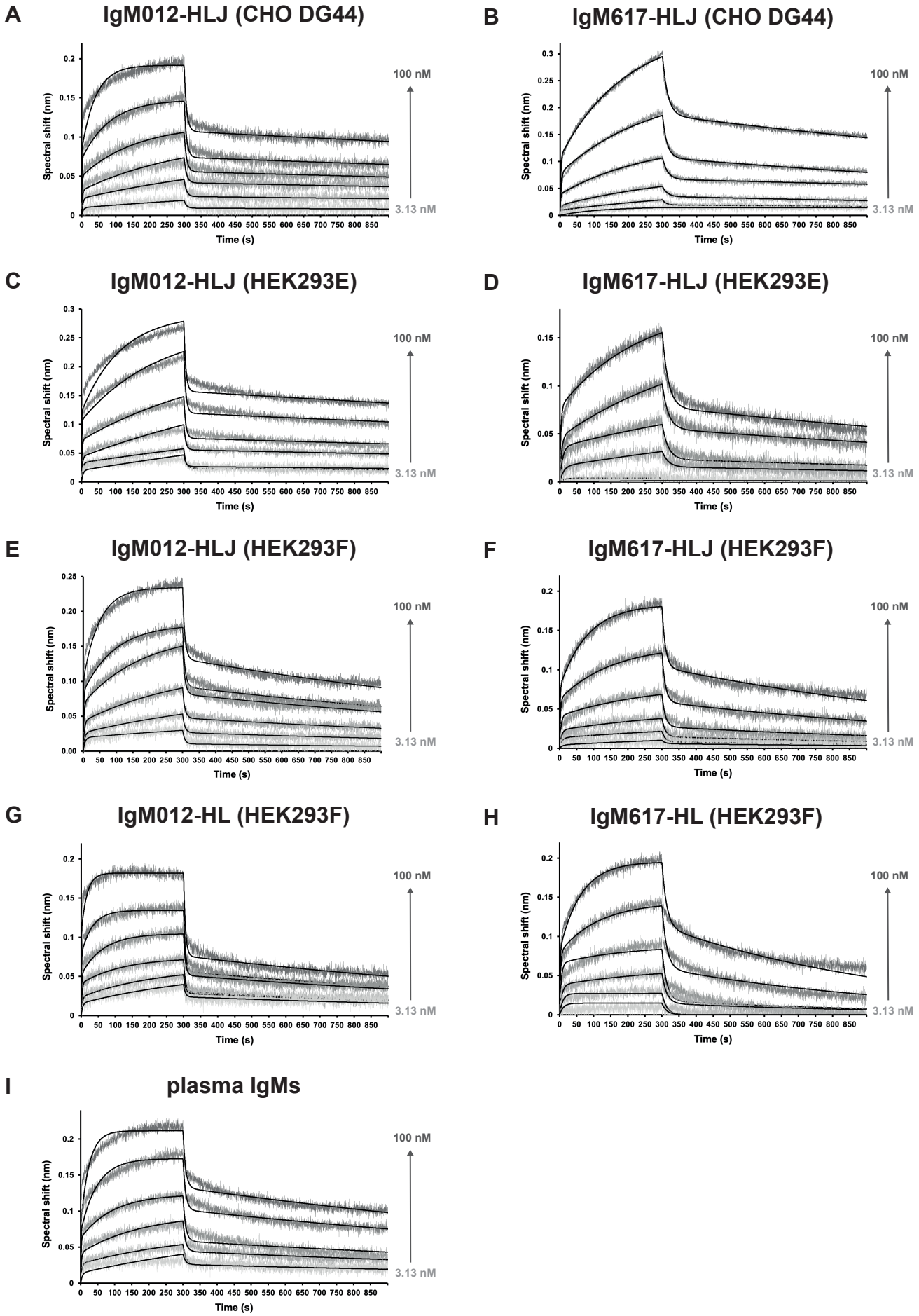
A
IgM012-HLJ (CHO DG44)
B
IgM617-HLJ (CHO DG44)
C
IgM012-HLJ (HEK293E)
D
IgM617-HLJ (HEK293E)
E
IgM012-HLJ (HEK293F)
F
IgM617-HLJ (HEK293F)
G
IgM012-HL (HEK293F)
H
IgM617-HL (HEK293F)
I
plasma IgMs
Spectral shift (nm)
Time (s)
100 nM
3.13 nM